

Evidence for a long-range component in the pion emission source in Au+Au collisions at $\sqrt{s_{NN}}=200$ GeV

S.S. Adler,⁵ S. Afanasiev,¹⁸ C. Aidala,⁵ N.N. Ajitanand,⁴⁴ Y. Akiba,^{21,39} J. Alexander,⁴⁴ R. Amirkas,¹³ L. Aphecetche,⁴⁶ S.H. Aronson,⁵ R. Auerbeck,⁴⁵ T.C. Awes,³⁶ R. Azmoun,⁴⁵ V. Babintsev,¹⁶ A. Baldisseri,¹⁰ K.N. Barish,⁶ P.D. Barnes,²⁸ B. Bassalleck,³⁴ S. Bathe,³¹ S. Batsouli,⁹ V. Baublis,³⁸ A. Bazilevsky,^{40,16} S. Belikov,^{17,16} Y. Berdnikov,⁴¹ S. Bhagavatula,¹⁷ J.G. Boissevain,²⁸ H. Borel,¹⁰ S. Borenstein,²⁶ M.L. Brooks,²⁸ D.S. Brown,³⁵ N. Bruner,³⁴ D. Bucher,³¹ H. Buesching,³¹ V. Bumazhnov,¹⁶ G. Bunce,^{5,40} J.M. Burward-Hoy,^{27,45} S. Butsyk,⁴⁵ X. Camard,⁴⁶ J.-S. Chai,¹⁹ P. Chand,⁴ W.C. Chang,² S. Chernichenko,¹⁶ C.Y. Chi,⁹ J. Chiba,²¹ M. Chiu,⁹ I.J. Choi,⁵³ J. Choi,²⁰ R.K. Choudhury,⁴ T. Chujo,⁵ P. Chung,⁴⁴ V. Cianciolo,³⁶ Y. Cobigo,¹⁰ B.A. Cole,⁹ P. Constantin,¹⁷ M. Csanád,¹² T. Csörgő,²² D. d'Enterria,⁴⁶ G. David,⁵ H. Delagrange,⁴⁶ A. Denisov,¹⁶ A. Deshpande,⁴⁰ E.J. Desmond,⁵ A. Devismes,⁴⁵ O. Dietzsch,⁴² O. Drapier,²⁶ A. Drees,⁴⁵ R. du Rietz,³⁰ A. Durum,¹⁶ D. Dutta,⁴ Y.V. Efremenko,³⁶ K. El Chenawi,⁵⁰ A. Enokizono,¹⁵ H. En'yo,^{39,40} S. Esumi,⁴⁹ L. Ewell,⁵ D.E. Fields,^{34,40} F. Fleuret,²⁶ S.L. Fokin,²⁴ B.D. Fox,⁴⁰ Z. Fraenkel,⁵² J.E. Frantz,⁹ A. Franz,⁵ A.D. Frawley,¹³ S.-Y. Fung,⁶ S. Garpman,^{30,*} T.K. Ghosh,⁵⁰ A. Glenn,⁴⁷ G. Gogiberidze,⁴⁷ M. Gonin,²⁶ J. Gosset,¹⁰ Y. Goto,⁴⁰ R. Granier de Cassagnac,²⁶ N. Grau,¹⁷ S.V. Greene,⁵⁰ M. Grosse Perdekamp,⁴⁰ W. Guryn,⁵ H.-Å. Gustafsson,³⁰ T. Hachiya,¹⁵ J.S. Haggerty,⁵ H. Hamagaki,⁸ A.G. Hansen,²⁸ E.P. Hartouni,²⁷ M. Harvey,⁵ R. Hayano,⁸ N. Hayashi,³⁹ X. He,¹⁴ M. Heffner,²⁷ T.K. Hemmick,⁴⁵ J.M. Heuser,⁴⁵ M. Hibino,⁵¹ J.C. Hill,¹⁷ W. Holzmann,⁴⁴ K. Homma,¹⁵ B. Hong,²³ A. Hoover,³⁵ T. Ichihara,^{39,40} V.V. Ikonnikov,²⁴ K. Imai,^{25,39} D. Isenhower,¹ M. Ishihara,³⁹ M. Issah,⁴⁴ A. Isupov,¹⁸ B.V. Jacak,⁴⁵ W.Y. Jang,²³ Y. Jeong,²⁰ J. Jia,⁴⁵ O. Jinnouchi,³⁹ B.M. Johnson,⁵ S.C. Johnson,²⁷ K.S. Joo,³² D. Jouan,³⁷ S. Kametani,^{8,51} N. Kamihara,^{48,39} J.H. Kang,⁵³ S.S. Kapoor,⁴ K. Katou,⁵¹ S. Kelly,⁹ B. Khachaturov,⁵² A. Khanzadeev,³⁸ J. Kikuchi,⁵¹ D.H. Kim,³² D.J. Kim,⁵³ D.W. Kim,²⁰ E. Kim,⁴³ G.-B. Kim,²⁶ H.J. Kim,⁵³ E. Kistenev,⁵ A. Kiyomichi,⁴⁹ K. Kiyoyama,³³ C. Klein-Boesing,³¹ H. Kobayashi,^{39,40} L. Kochenda,³⁸ V. Kochetkov,¹⁶ D. Koehler,³⁴ T. Kohama,¹⁵ M. Kopytine,⁴⁵ D. Kotchetkov,⁶ A. Kozlov,⁵² P.J. Kroon,⁵ C.H. Kuberg,^{1,28,*} K. Kurita,⁴⁰ Y. Kuroki,⁴⁹ M.J. Kweon,²³ Y. Kwon,⁵³ G.S. Kyle,³⁵ R. Lacey,⁴⁴ V. Ladygin,¹⁸ J.G. Lajoie,¹⁷ A. Lebedev,^{17,24} S. Leckey,⁴⁵ D.M. Lee,²⁸ S. Lee,²⁰ M.J. Leitch,²⁸ X.H. Li,⁶ H. Lim,⁴³ A. Litvinenko,¹⁸ M.X. Liu,²⁸ Y. Liu,³⁷ C.F. Maguire,⁵⁰ Y.I. Makdisi,⁵ A. Malakhov,¹⁸ V.I. Manko,²⁴ Y. Mao,^{7,39} G. Martinez,⁴⁶ M.D. Marx,⁴⁵ H. Masui,⁴⁹ F. Matathias,⁴⁵ T. Matsumoto,^{8,51} P.L. McGaughey,²⁸ E. Melnikov,¹⁶ F. Messer,⁴⁵ Y. Miake,⁴⁹ J. Milan,⁴⁴ T.E. Miller,⁵⁰ A. Milov,^{45,52} S. Mioduszewski,⁵ R.E. Mischke,²⁸ G.C. Mishra,¹⁴ J.T. Mitchell,⁵ A.K. Mohanty,⁴ D.P. Morrison,⁵ J.M. Moss,²⁸ F. Mühlbacher,⁴⁵ D. Mukhopadhyay,⁵² M. Muniruzzaman,⁶ J. Murata,^{39,40} S. Nagamiya,²¹ J.L. Nagle,⁹ T. Nakamura,¹⁵ B.K. Nandi,⁶ M. Nara,⁴⁹ J. Newby,⁴⁷ P. Nilsson,³⁰ A.S. Nyanin,²⁴ J. Nystrand,³⁰ E. O'Brien,⁵ C.A. Ogilvie,¹⁷ H. Ohnishi,^{5,39} I.D. Ojha,^{50,3} K. Okada,³⁹ M. Ono,⁴⁹ V. Onuchin,¹⁶ A. Oskarsson,³⁰ I. Otterlund,³⁰ K. Oyama,⁸ K. Ozawa,⁸ D. Pal,⁵² A.P.T. Palounek,²⁸ V. Pantuev,⁴⁵ V. Papavassiliou,³⁵ J. Park,⁴³ A. Parmar,³⁴ S.F. Pate,³⁵ T. Peitzmann,³¹ J.-C. Peng,²⁸ V. Peresedov,¹⁸ C. Pinkenburg,⁵ R.P. Pisani,⁵ F. Plasil,³⁶ M.L. Purschke,⁵ A.K. Purwar,⁴⁵ J. Rak,¹⁷ I. Ravinovich,⁵² K.F. Read,^{36,47} M. Reuter,⁴⁵ K. Reygers,³¹ V. Riabov,^{38,41} Y. Riabov,³⁸ G. Roche,²⁹ A. Romana,^{26,*} M. Rosati,¹⁷ P. Rosnet,²⁹ S.S. Ryu,⁵³ M.E. Sadler,¹ N. Saito,^{39,40} T. Sakaguchi,^{8,51} M. Sakai,³³ S. Sakai,⁴⁹ V. Samsonov,³⁸ L. Sanfratello,³⁴ R. Santo,³¹ H.D. Sato,^{25,39} S. Sato,^{5,49} S. Sawada,²¹ Y. Schutz,⁴⁶ V. Semenov,¹⁶ R. Seto,⁶ M.R. Shaw,^{1,28} T.K. Shea,⁵ T.-A. Shibata,^{48,39} K. Shigaki,^{15,21} T. Shiina,²⁸ C.L. Silva,⁴² D. Silvermyr,^{28,30} K.S. Sim,²³ C.P. Singh,³ V. Singh,³ M. Sivertz,⁵ A. Soldatov,¹⁶ R.A. Soltz,²⁷ W.E. Sondheim,²⁸ S.P. Sorensen,⁴⁷ I.V. Sourikova,⁵ F. Staley,¹⁰ P.W. Stankus,³⁶ E. Stenlund,³⁰ M. Stepanov,³⁵ A. Ster,²² S.P. Stoll,⁵ T. Sugitate,¹⁵ J.P. Sullivan,²⁸ E.M. Takagui,⁴² A. Taketani,^{39,40} M. Tamai,⁵¹ K.H. Tanaka,²¹ Y. Tanaka,³³ K. Tanida,³⁹ M.J. Tannenbaum,⁵ A. Taranenko,⁴⁴ P. Tarján,¹¹ J.D. Tepe,^{1,28} T.L. Thomas,³⁴ J. Tojo,^{25,39} H. Torii,^{25,39} R.S. Towell,¹ I. Tseruya,⁵² H. Tsuruoka,⁴⁹ S.K. Tuli,³ H. Tydesjö,³⁰ N. Tyurin,¹⁶ H.W. van Hecke,²⁸ J. Velkovska,^{5,45} M. Velkovsky,⁴⁵ V. Veszprémi,¹¹ L. Villatte,⁴⁷ A.A. Vinogradov,²⁴ M.A. Volkov,²⁴ E. Vznuzdaev,³⁸ X.R. Wang,¹⁴ Y. Watanabe,^{39,40} S.N. White,⁵ F.K. Wohn,¹⁷ C.L. Woody,⁵ W. Xie,⁶ Y. Yang,⁷ A. Yanovich,¹⁶ S. Yokkaichi,^{39,40} G.R. Young,³⁶ I.E. Yushmanov,²⁴ W.A. Zajc,^{9,†} C. Zhang,⁹ S. Zhou,⁷ S.J. Zhou,⁵² and L. Zolin¹⁸

(PHENIX Collaboration)

¹Abilene Christian University, Abilene, TX 79699, U.S.

²Institute of Physics, Academia Sinica, Taipei 11529, Taiwan

³Department of Physics, Banaras Hindu University, Varanasi 221005, India

⁴Bhabha Atomic Research Centre, Bombay 400 085, India

- ⁵Brookhaven National Laboratory, Upton, NY 11973-5000, U.S.
⁶University of California - Riverside, Riverside, CA 92521, U.S.
⁷China Institute of Atomic Energy (CIAE), Beijing, People's Republic of China
⁸Center for Nuclear Study, Graduate School of Science, University of Tokyo, 7-3-1 Hongo, Bunkyo, Tokyo 113-0033, Japan
⁹Columbia University, New York, NY 10027 and Nevis Laboratories, Irvington, NY 10533, U.S.
¹⁰Dapnia, CEA Saclay, F-91191, Gif-sur-Yvette, France
¹¹Debrecen University, H-4010 Debrecen, Egyetem tér 1, Hungary
¹²ELTE, Eötvös Loránd University, H - 1117 Budapest, Pázmány P. s. 1/A, Hungary
¹³Florida State University, Tallahassee, FL 32306, U.S.
¹⁴Georgia State University, Atlanta, GA 30303, U.S.
¹⁵Hiroshima University, Kagamiyama, Higashi-Hiroshima 739-8526, Japan
¹⁶IHEP Protvino, State Research Center of Russian Federation, Institute for High Energy Physics, Protvino, 142281, Russia
¹⁷Iowa State University, Ames, IA 50011, U.S.
¹⁸Joint Institute for Nuclear Research, 141980 Dubna, Moscow Region, Russia
¹⁹KAERI, Cyclotron Application Laboratory, Seoul, South Korea
²⁰Kangnung National University, Kangnung 210-702, South Korea
²¹KEK, High Energy Accelerator Research Organization, Tsukuba, Ibaraki 305-0801, Japan
²²KFKI Research Institute for Particle and Nuclear Physics of the Hungarian Academy of Sciences (MTA KFKI RMKI), H-1525 Budapest 114, POBox 49, Budapest, Hungary
²³Korea University, Seoul, 136-701, Korea
²⁴Russian Research Center "Kurchatov Institute", Moscow, Russia
²⁵Kyoto University, Kyoto 606-8502, Japan
²⁶Laboratoire Leprince-Ringuet, Ecole Polytechnique, CNRS-IN2P3, Route de Saclay, F-91128, Palaiseau, France
²⁷Lawrence Livermore National Laboratory, Livermore, CA 94550, U.S.
²⁸Los Alamos National Laboratory, Los Alamos, NM 87545, U.S.
²⁹LPC, Université Blaise Pascal, CNRS-IN2P3, Clermont-Fd, 63177 Aubiere Cedex, France
³⁰Department of Physics, Lund University, Box 118, SE-221 00 Lund, Sweden
³¹Institut für Kernphysik, University of Muenster, D-48149 Muenster, Germany
³²Myongji University, Yongin, Kyonggido 449-728, Korea
³³Nagasaki Institute of Applied Science, Nagasaki-shi, Nagasaki 851-0193, Japan
³⁴University of New Mexico, Albuquerque, NM 87131, U.S.
³⁵New Mexico State University, Las Cruces, NM 88003, U.S.
³⁶Oak Ridge National Laboratory, Oak Ridge, TN 37831, U.S.
³⁷IPN-Orsay, Université Paris Sud, CNRS-IN2P3, BP1, F-91406, Orsay, France
³⁸PNPI, Petersburg Nuclear Physics Institute, Gatchina, Leningrad region, 188300, Russia
³⁹RIKEN, The Institute of Physical and Chemical Research, Wako, Saitama 351-0198, Japan
⁴⁰RIKEN BNL Research Center, Brookhaven National Laboratory, Upton, NY 11973-5000, U.S.
⁴¹Saint Petersburg State Polytechnic University, St. Petersburg, Russia
⁴²Universidade de São Paulo, Instituto de Física, Caixa Postal 66318, São Paulo CEP05315-970, Brazil
⁴³System Electronics Laboratory, Seoul National University, Seoul, South Korea
⁴⁴Chemistry Department, Stony Brook University, SUNY, Stony Brook, NY 11794-3400, U.S.
⁴⁵Department of Physics and Astronomy, Stony Brook University, SUNY, Stony Brook, NY 11794, U.S.
⁴⁶SUBATECH (Ecole des Mines de Nantes, CNRS-IN2P3, Université de Nantes) BP 20722 - 44307, Nantes, France
⁴⁷University of Tennessee, Knoxville, TN 37996, U.S.
⁴⁸Department of Physics, Tokyo Institute of Technology, Oh-okayama, Meguro, Tokyo, 152-8551, Japan
⁴⁹Institute of Physics, University of Tsukuba, Tsukuba, Ibaraki 305, Japan
⁵⁰Vanderbilt University, Nashville, TN 37235, U.S.
⁵¹Waseda University, Advanced Research Institute for Science and Engineering, 17 Kikui-cho, Shinjuku-ku, Tokyo 162-0044, Japan
⁵²Weizmann Institute, Rehovot 76100, Israel
⁵³Yonsei University, IPAP, Seoul 120-749, Korea

(Dated: July 14, 2018)

Emission source functions are extracted from correlation functions constructed from charged pions produced at mid-rapidity in Au+Au collisions at $\sqrt{s_{NN}}=200$ GeV. The source parameters extracted from these functions at low k_T , give first indications of a long tail for the pion emission source. The source extension cannot be explained solely by simple kinematic considerations. The possible role of a halo of secondary pions from resonance emissions is explored.

PACS numbers: 25.75.Ld, 25.75.Dw

Collisions between ultra-relativistic heavy ions can lead to extremely high energy-density nuclear matter [1].

The decay dynamics of this matter are strongly influenced by the nuclear Equation of State (EOS) and possi-

bly by a de-confined phase [2]. An emitting system which undergoes a strong first order phase transition is expected to show a much larger space-time extent than would be expected if the system remained in the hadronic phase throughout the collision process [3]. Indeed, several hydrodynamical calculations show such an increase for particle emission sources [3, 4], providing hadronization does not occur via a supercooled state [5]. It has also been suggested that the shape of the emission source function can provide signals for a second order phase transition and whether or not particle emission occurs near to the critical end point in the QCD phase diagram [6].

Interferometry studies provide important information on the emission source function for particles produced in nuclear reactions ranging from elementary collisions (e^+e^- and $(\bar{p})pp$) to those involving very heavy ions [7, 8, 9]. Recent studies include the use of two- and three-pion interferometry correlations spanning the beam energies of the Alternating Gradient Synchrotron (AGS), the Super Proton Synchrotron (SPS) and the Relativistic Heavy Ion Collider (RHIC) ($\sqrt{s_{NN}} \sim 2 - 200$ GeV) [10, 11, 12, 13].

A common theme for these papers is the extraction of the widths of emission source functions which are assumed to be Gaussian. For such extractions, the Coulomb effects on the correlation function are usually assumed to be separable [14] as well. Such an approach was followed in an earlier analysis in which we used the Bowler-Sinyukov 3D HBT analysis method [in Bertsch-Pratt coordinates] to probe for long-range emissions from a possible long-lived source [15]. The RMS-widths so obtained for each dimension of the source R_{long} , R_{side} and R_{out} , gave no evidence for such emissions, suggesting that the sound speed is not zero during an extended hadronization period.

In this letter we exploit the model-independent imaging technique of Brown and Danielewicz [16, 17] to make a more detailed study of both the shape and the space-time characteristics of the pion emission source function. The method uses a numerical calculation of the two particle wave function (including final state interactions (FSI)) to produce an inversion matrix that operates on the correlation function to produce the corresponding source function. The technique has been used to address only a few data sets [18, 19] at relativistic beam energies.

The measurements were made with the PHENIX detector [20] at RHIC. The charged pions relevant to this analysis were detected in the two central arms ($|\eta| \leq 0.35$). Track reconstruction was accomplished via pattern recognition using the drift chamber (DC) followed by two layers of multi-wire proportional chambers with pad readout located at radii of 2, 2.5, and 5 m [20]. Particle momenta were measured with the resolution $\delta p/p = 0.7\% \oplus 1.0\%p$ (GeV/c). Very good pion identification (PID) was achieved with a 2σ cut about the pion peak in the squared-mass distribution for $p_T \lesssim 2.0$ GeV/c and $p_T \lesssim 1$ GeV/c in the Time

of Flight (TOF) and the Electromagnetic Calorimeter (EMC) respectively. The event centrality was determined using the PHENIX beam-beam counter and the zero degree calorimeter [21]. Approximately 22 million Au+Au events were analyzed to generate and study correlation functions for several centrality and p_T selections.

Two-pion interferometry correlations were obtained via the correlation function $C(q) = N_{\text{cor}}(q)/N_{\text{mix}}(q)$, where the numerator is the relative momentum distribution of particle pairs from the same event (foreground pairs) and the denominator is the relative momentum distribution of particle pairs obtained from mixed events (background pairs). Here, $q = \frac{1}{2}\sqrt{-(p_1 - p_2)^2}$ is half of the relative momentum between the two particles in the pair c.m. frame (PCMS). p_1 and p_2 are the momentum 4-vectors of each particle in the pair and $C(q) \equiv 1$ for large q -values where final-state interactions are negligible. Track-pair cuts similar to those of Ref. [12] were applied to foreground and background pairs respectively. That is, pairs within 0-5 cm in the beam direction (ΔZ_{DC}) and 0.02 radians in azimuthal angle ($\Delta\phi_{DC}$) in the DC were eliminated from the pair sample to remove ghost tracks, and pairs within $0.0 < \Delta\phi_{DC} < 0.1$ radians for $\Delta Z_{DC} > 5$ cm were removed to avoid an inefficient region. The latter set of cuts were supplemented with the removal of pairs having a separation $\Delta R \leq 14$ cm and ≤ 16 cm in the TOF and EMC respectively. Systematic variations of all of these cuts were explored to determine systematic error estimates; very little influence on the extracted correlation functions was found. Careful studies of the influence of momentum resolution on the correlation function were also made following the simulation technique outlined in Ref. [12]. The maximum effect was found to be $\sim 0.4\%$ change in the correlation function at low q values, so it was neglected.

The filled circles in Fig. 1(a) show the one-dimensional (1D) correlation function $C(q)$, for a centrality of 0 - 20% and for $0.20 < k_T = \frac{1}{2}(p_{T,1} + p_{T,2}) < 0.36$ GeV/c. The characteristic enhancement for $q \lesssim 25$ MeV/c reflects a combination of Bose-Einstein statistics and the FSI between pion pairs. The correlation function is not Coulomb corrected because the FSI (including Coulomb but no strong interaction) is included in the imaging and fitting procedure as described below.

The 1D correlation function and source function $S(r)$ (the probability of emitting a pair of particles at a separation r in the PCMS frame), are related via the 1D Koonin-Pratt equation [22]:

$$C(q) - 1 = 4\pi \int dr r^2 K_0(q, r) S(r). \quad (1)$$

The angle-averaged kernel $K_0(q, r)$ encodes the FSI and is given in terms of the final state wave function $\Phi_{\mathbf{q}}(\mathbf{r})$, as $K_0(q, r) = \frac{1}{2} \int d(\cos(\theta_{\mathbf{q}, \mathbf{r}})) (|\Phi_{\mathbf{q}}(\mathbf{r})|^2 - 1)$, where $\theta_{\mathbf{q}, \mathbf{r}}$ is the angle between \mathbf{q} and \mathbf{r} [17]. The procedure for the inversion of Eq. 1 to obtain $S(r)$ is also given in Ref. [17].

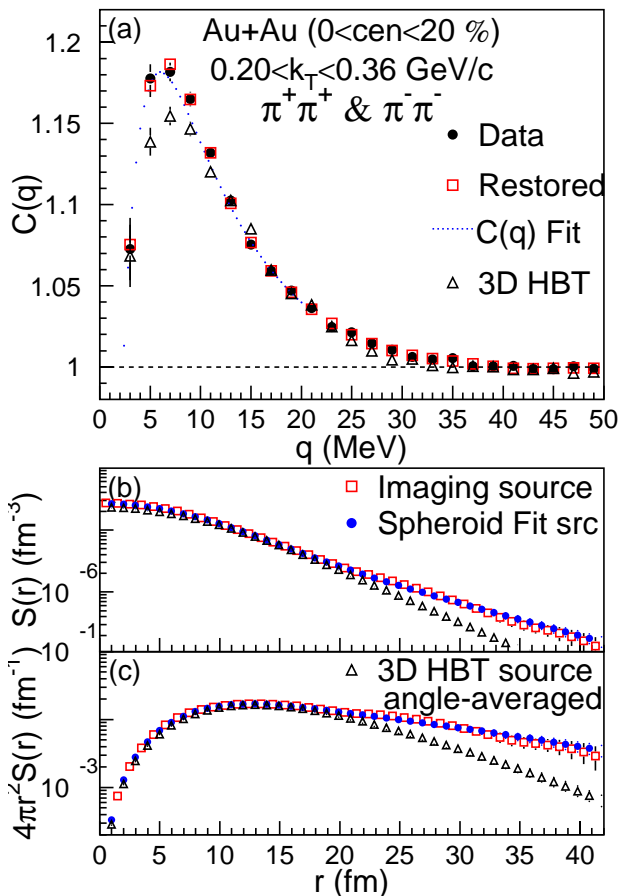


FIG. 1: (color online) (upper, a) (filled circles) Correlation function, $C(q)$ for $\pi^+\pi^+$ and $\pi^-\pi^-$ pairs; (open squares) restored correlation from imaging technique; (dotted line) direct correlation fitting; (open triangles) 1D angle-averaged correlation of 3D correlation function. (lower) 1D source function (b) $S(r)$ and (c) $4\pi r^2 S(r)$: (open squares) imaging; (filled circles) spheroid fit to correlation function; (open triangles) angle-averaging of 3D-Gaussian source function. Systematic errors are less than size of data points.

The open squares in Fig. 1(b) show the source function obtained from the correlation function presented in Fig. 1(a). As a cross check of the imaging procedure, a restored correlation function was generated via Eq. 1 with the extracted source function as input. The open squares and filled circles in Fig. 1(a) indicate excellent consistency between the measured and restored correlation functions. The 1D-source function (cf. Fig. 1(b)) points to a Gaussian-like pattern at small r and a previously unresolved “tail” at large r . The robustness of this tail was established via an extensive array of tests including its dependence on pair and PID cuts, and on momentum resolution; no variation outside of the stated error bars was found.

This new observation of a tail is made more transparent via a comparison with the source function con-

structed from the parameters (R_{long} , R_{side} , R_{out} and λ), obtained in an earlier 3D HBT analysis [15]. The procedures outlined in Ref.[17] were employed to construct this source function (see Fig. 1). The measured and 3D angle-averaged correlation functions differ for $q \lesssim 15$ MeV/c as do the respective source functions for $r \gtrsim 17$ fm. The imaged source function exhibits a more prominent tail than the angle averaged 3D HBT source function. This difference could stem from the Gaussian shape assumption employed in the 3D HBT analysis. The 3D Gaussian fitting procedure by construction is sensitive only to the main component of $S(r)$, and thus would not be capable of resolving fine structure at small- q /large- r . Given the fact that the volume element increases quadratically with pair separation, this difference is considerable as shown in Fig.1(c), where the radial probabilities ($4\pi r^2 S(r)$) are compared. The open triangles in Fig. 1(a) clearly indicate that the differences in the source functions reflect an important disparity in the corresponding correlation functions for $q \lesssim 10 - 15$ MeV.

Parameters of the source function for different assumed shapes were extracted via direct fits to the correlation function. Filled circles in Figs. 1(b,c) show the source function obtained from such a fit for a Spheroidal shape [17],

$$S(r) = \frac{\lambda R_{\text{eff}} \times e^{-\frac{r^2}{4R_{\text{eff}}^2}} \text{erfi}\left(\frac{r}{2R_{\text{eff}}}\right)}{(8\pi R_T^2 R_0 r)}, \text{ for } R_0 > R_T, \quad (2)$$

where $R_{\text{eff}} = 1/\sqrt{(1/R_T^2 - 1/R_0^2)}$, R_T is the radius of the Spheroid in two perpendicular spatial dimensions and $R_0 = a \times R_T$ is the radius in the third spatial dimension; a is a scale factor. The long axis of the Spheroid is assumed to be oriented in the out direction of the Bertsch-Pratt coordinate system. The fraction of pion pairs which contribute to the source λ , is given by the integral of the normalized source function over the full range of r .

The procedure for making a direct fit to the correlation function involves the determination of a set of values for the Spheroid parameters of Eq. 2, which reproduce the observed correlation function when the resulting source function is inserted into Eq. 1. The minimization package MINUIT was used to minimize the χ^2 between the observed and calculated correlation function. The χ^2/ndf value so obtained was ~ 1 . The dotted curve in Fig. 1(a) shows the fit to the data. The resulting source function shown in Figs. 1(b) and 1(c), indicates very good agreement with that obtained via the imaging technique. This shape parametrization is not unique; an essentially indistinguishable source was also obtained for a fit performed with a Gaussian plus modified exponential [23] shape. The simpler Spheroid parametrization was chosen for the discussion below.

The Spheroidal source function (Eq. 2) can be approx-

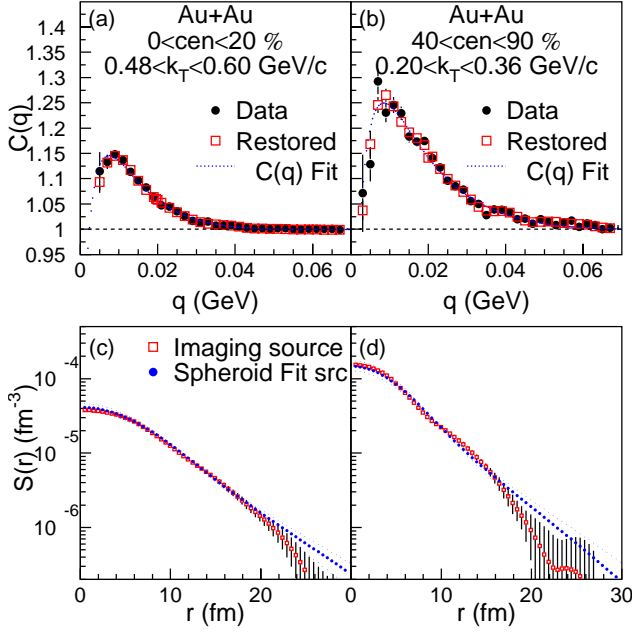


FIG. 2: (color online) (upper) Correlation functions, $C(q)$, for $\pi^+\pi^+$ and $\pi^-\pi^-$ pairs and (lower) corresponding source functions, $S(r)$ for (a, c) high k_T most central collisions; (b, d) low k_T peripheral collisions. Error bars indicate statistical errors with symbols as in Fig. 1.

imated by a short-range Gaussian source $S_{sr}(r)$;

$$S_{sr}(r) \sim \lambda e^{-r^2 \left[\frac{1}{6R_T^2} + \frac{1}{12R_0^2} \right]} / (8\pi\sqrt{\pi}R_T^2R_0), \quad (3)$$

for small r , and a long-range source $S_{lr}(r)$ for $r \gg 2R_T R_0 / \sqrt{R_0^2 - R_T^2}$ given by

$$S_{lr}(r) \sim \lambda R_0 e^{-r^2/4R_0^2} / (4\pi\sqrt{\pi}(R_0^2 - R_T^2)r^2). \quad (4)$$

Thus, the emission source shown in Figs. 1(b) and 1(c) can be interpreted to reflect a short range Gaussian source of radius $R_{sr} = \sqrt{3R_T^2 R_0^2 / (2R_0^2 + R_T^2)}$ and a long-range tail of extended space-time extent $R_{lr} = R_0$. The fraction of pairs associated with these sources $\lambda_{sr} = \lambda a^2 (3/(2a^2 + 1))^{3/2}$ and $\lambda_{lr} = (\lambda - \lambda_{sr})$, are obtained from Eq. 3 and the conservation of pairs respectively.

Source functions were extracted via imaging and spheroid fits for several k_T and centrality selections, in order to map the regions in k_T and centrality where the long-range tail is prominent. Representative results are shown in Fig.2 for the indicated cuts. The experimental and restored correlation functions, compared in Figs.2(a,b), indicate good agreement consistent within the statistics, as do the corresponding source functions shown in Figs.2(c,d).

Figure 3 gives a more complete summary of the extracted source parameters. The indicated systematic errors were obtained by varying the pair cuts in the analysis. The centrality and k_T dependence of the RMS radius

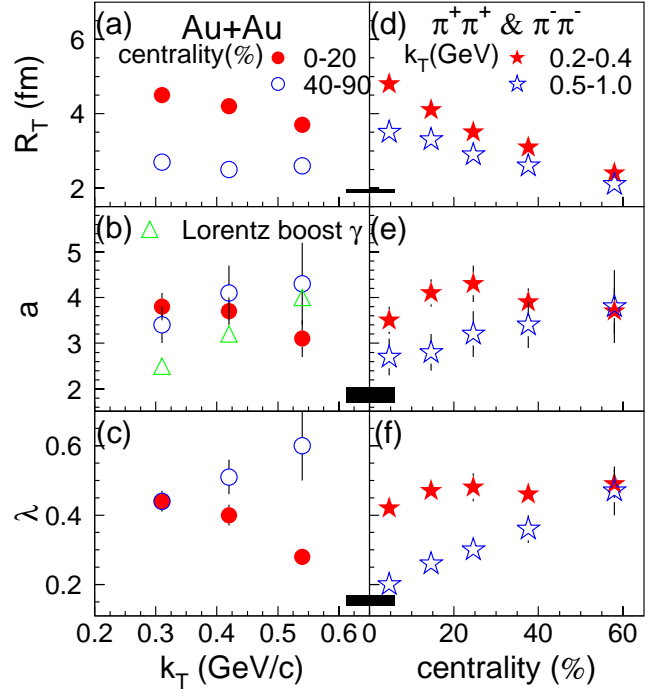


FIG. 3: (color online) (left) k_T dependence of extracted spheroidal source parameters for pion source functions (a) R_T , (b) a , and (c) λ for (filled circles) most central collisions; (open circles) peripheral collisions. (right) centrality dependence of same parameters for (filled stars) low k_T (0.2–0.4 GeV/c); (open stars) high k_T (0.5–1.0 GeV/c). Filled bands indicate systematic errors.

of the short-range source R_{sr} , is similar (within 10%) to that obtained for R_{long} and R_{side} in an earlier analysis [15] (cf. Figs. 3 (a) and (d)). The long-range source shows an effective radius $R_{lr} = a \times R_T$, which is 3-4 times R_T (cf. Figs. 3 (b) and (e)) with the largest values for low k_T and the most central collisions. The fraction of pairs exhibiting these characteristics is given by the λ values shown in Figs. 3 (c, f); maximum prominence is shown for low k_T pairs from central collisions.

A central question is the origin of the long-range contribution to the emitting source. Instantaneous freeze-out of an isotropic source in the longitudinal co-moving system (LCMS) would give $R_{lr} = R_{out} = \gamma \times R_T$ in the PCMS. Thus, the values for a and γ , shown in Fig. 3(b), can be directly compared. At low k_T , γ is seen to be significantly less than a . Thus, a simple kinematic transformation from the LCMS to PCMS can not account for the observed source parameters at this k_T .

Could a composite particle emission source comprised of a central core and a halo of long-lived resonances account for the observations? For such emissions, the pairing between pions from the core and secondary pions from the halo is expected to dominate the long-range emissions [24]. If it is assumed that this halo includes only ω decay ($c\tau \sim 24$ fm), one may compare the ω yield with a simple

estimate of the fraction of pion pairs associated with the short- and long-range sources. Using the a and γ values in Fig. 3(b), $\lambda_{sr} \sim 0.22 - 0.32$, $\lambda_{lr} \sim 0.23 - 0.13$ and $\lambda_{lr}/\lambda_{sr} \sim 0.4 - 1.0$ for the lowest k_T . The preliminary data for $\omega/\pi^- = 0.1$ from Ref. [25] gives an estimate for $\lambda_{lr}/\lambda_{sr} \sim 2 \times 0.1/\sqrt{\lambda_{sr}} \sim 0.35 - .43$ which lies at the lower end of the estimates obtained from the source parameters. Therefore, it is plausible that a maximal kinematic boost combined with a halo of ω s could account for $\lambda_{lr}/\lambda_{sr}$. However, the steep centrality dependence of the radius of the long range source inferred from Figs. 3(d,e) is not compatible with what would be expected for significant ω resonance contribution. Also, initial comparisons to the results from a recent dynamical model calculation [26] indicate that resonance emissions are not sufficient to fully account for the observed tails in the source functions.

In summary, we have made the first extraction of the full 1D emission source function for pions in Au+Au collisions at RHIC ($\sqrt{s_{NN}} = 200$ GeV). This source function points to separate but prominent contributions from short-range emissions and a long-range tail of larger space-time extent than has been previously observed. This tail cannot be explained solely by simple kinematic considerations associated with a frame transformation from the LCMS to the PCMS. Further detailed 3D imaging measurements in conjunction with in depth model studies, are required to quantitatively pin down the origin of this tail and to determine whether or not it is related to a phase transition.

* Deceased

† PHENIX Spokesperson:zajc@nevis.columbia.edu

- [1] K. Adcox et al., Nucl. Phys. **A757**, 184 (2005).
- [2] E. V. Shuryak, Nucl. Phys. **A750**, 64 (2005).
- [3] S. Pratt, Phys. Rev. Lett. **53**, 1219 (1984).
- [4] D. Teaney et al., Phys. Rev. Lett. **86**, 4783 (2001).
- [5] T. Csorgo et al., Phys. Lett. **B333**, 494 (1994).
- [6] T. Csorgo, S. Hegyi, T. Novak, and W. A. Zajc (2005), nucl-th/0512060.
- [7] E. V. Shuryak, Phys. Lett. **B44**, 387 (1973).
- [8] U. Heinz et al., Ann. Rev. Nucl. Part. Sci. **49**, 529 (1999).
- [9] T. Csorgo, Heavy Ion Phys. **15**, 1 (2002).
- [10] M. A. Lisa et al., Annu. Rev. Nucl. Part. Sci. **55**, 357 (2005).
- [11] C. Adler et al., Phys. Rev. Lett. **87**, 082301 (2001).
- [12] K. Adcox et al., Phys. Rev. Lett. **88**, 192302 (2002).
- [13] J. Adams et al., Phys. Rev. Lett. **91**, 262301 (2003).
- [14] Y. Sinyukov et al., Phys. Lett. **B432**, 248 (1998).
- [15] S. S. Adler et al., Phys. Rev. Lett. **93**, 152302 (2004).
- [16] D. A. Brown et al., Phys. Lett. **B398**, 252 (1997).
- [17] D. A. Brown et al., Phys. Rev. **C64**, 014902 (2001).
- [18] S. Y. Panitkin et al., Phys. Rev. Lett. **87**, 112304 (2001).
- [19] P. Chung et al., Phys. Rev. Lett. **91**, 162301 (2003).
- [20] K. Adcox et al., Nucl. Instrum. Meth. **A499**, 469 (2003).
- [21] K. Adcox et al., Phys. Rev. **C69**, 024904 (2004).
- [22] S. E. Koonin, Phys. Lett. **B70**, 43 (1977).
- [23] P. Chung et al., Nucl. Phys. **A749**, 275 (2005).
- [24] S. Nickerson et al., Phys. Rev. **C57**, 3251 (1998).
- [25] W. Broniowski et al., Acta Phys. Hung. **A22**, 159 (2005).
- [26] A. Kisiel, W. Florkowski, and W. Broniowski (2006), nucl-th/0602039.